Spin fluctuations in itinerant magnets

B D Rainford

University of Southampton, England

1 Introduction

Advances in the theory of spin fluctuations have resulted in a remarkable synthesis of the microscopic spin dynamics and the bulk properties of weak ferromagnets and exchange enhanced paramagnets. In the case of systems like YMn_2 and β-Mn, which display antiferromagnetic spin fluctuations, it appears that topological frustration is an important extra factor, leading to quantum spin liquid behaviour. Inelastic neutron scattering and μSR have important and complementary roles in characterising the spin dynamics in these intriguing magnetic materials.

The very simplest approach to itinerant magnetism is the one-band Hubbard model:

$$H = \sum_k E_k n_k + \sum_i U n_i(\uparrow) n_i(\downarrow)$$

where n_k, n_i are fermion number operators for a Bloch state with wavevector k and a Wannier state at site i respectively. The first term represents the band energies of the itinerant electrons and the second term is the coulomb energy between electrons of opposite spin in the electron orbital on site i. The coulomb term is the largest of the many types of correlation between electrons in a metal: it acts only between electrons of opposite spins because of the Pauli exclusion principle. Consequently it results in an effective attractive interaction between electrons of parallel spin. A mean field treatment of this Hamiltonian, in the spirit of the random phase approximation (RPA—see for example White, 1983) leads to the standard result for the dynamical susceptibility:

$$\chi(q,\omega) = \frac{\chi_0(q,\omega)}{1 - I\chi_0(q,\omega)}$$

where $I = 2U/(g\mu_B)^2$. The "bare" susceptibility $\chi_0(q,\omega)$ of the electrons is given by

$$\chi_0(q,\omega) = \lim_{\epsilon \to 0} \sum_k \frac{\langle n_{k+q} \rangle - \langle n_k \rangle}{E_{k+q} - E_k - \hbar\omega - i\epsilon} \qquad (1)$$

which can be calculated from the band structure. For paramagnets like Pd, the uniform susceptibility is perhaps 5–10 times larger than that calculated from the Pauli band susceptibility. This is a consequence of the "exchange enhancement" resulting from the electron correlations:

$$\chi(0,0) = \frac{\chi_0(0,0)}{1 - I\chi_0(0,0)}. \tag{2}$$

Clearly if the exchange enhancement is large enough, the denominator in (2) can approach zero, and the susceptibility then diverges when

$$I\chi_0(0,0) = 1,$$

signalling the onset of a phase transition to a ferromagnetic ground state. This condition is a version of the Stoner criterion. The form of the dynamical susceptibility for exchange enhanced paramagnets, (Doniach 1967) is shown in Figure 1 as a function of $\alpha = I\chi_0(0,0)$. The imaginary part of the susceptibility has been shown since it is this property which is measured by inelastic neutron scattering, and also determines the μSR relaxation rate. It can be seen that close to the onset of ferromagnetism most of the weight in the response occurs at low frequencies. This response corresponds to the spectrum of long-lived spin fluctuations, which are electron-hole pairs correlated by the effective attraction of parallel spins arising from the coulomb repulsion and exchange correlations. The fluctuation-dissipation theorem tells us that the mean square amplitude of the spin fluctuations is given by:

$$\langle m_\nu^2 \rangle = \frac{4\hbar}{V} \sum_{q,\omega} n(\omega) \operatorname{Im} \chi_\nu(q,\omega), \tag{3}$$

i.e. the integrated area under the curves in Figure 1, weighted by the detailed balance factor $n(\omega) = [\exp(\hbar\omega/k_B T) - 1]^{-1}$.

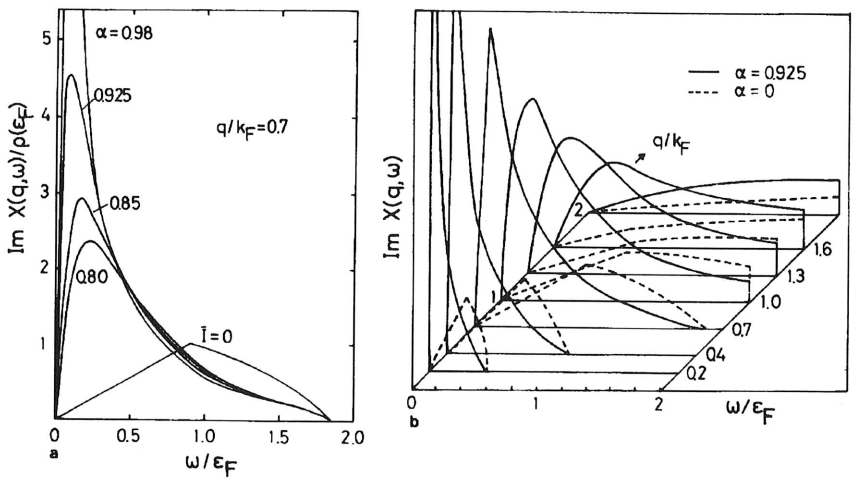

Figure 1. *Imaginary part of dynamical susceptibility of an electron gas (Doniach 1967): (a) for one particular wavevector $q = 0.7k_F$ with varying degrees of exchange enhancement α and (b) the q, ω dependence of the response for $\alpha = 0.925$.*

Modern band calculations are based on "spin density functional" theory where the effective potential in which the electrons move and the exchange-correlation potential are written as functionals of the spin up and spin down electron densities $n(\uparrow, \mathbf{r})$, $n(\downarrow, \mathbf{r})$. Band structures can be calculated self-consistently, so that ground state quantities such as the lattice parameter, the cohesive energy and the magnetic moment can be estimated starting only from the atomic number and an assumed crystal structure. The accuracy of such estimates is remarkably good: for an elemental metal typically the lattice parameter is correct to a few percent, while the bulk modulus and magnetic moment are perhaps within 10% of the observed values. The estimated ground state energy is usually accurate enough to distinguish ferromagnetic and antiferromagnetic states. However the properties which we would predict for itinerant magnets at finite temperature, on the basis of the band structure ("Stoner theory") are often in very poor agreement with experiment. In particular the predicted value of the ordering temperature T_C is typically much too high and the temperature dependence of the susceptibility in the paramagnetic state is quite different from experiment. This is seen readily by making a Landau-Ginzberg expansion of the free energy as a function of the magnetisation:

$$\frac{F(M)}{V} = \frac{F_0(0)}{V} + \frac{aM^2}{2} + \frac{bM^4}{4} - \frac{IM^2}{2} + \cdots \tag{4}$$

where the last term represents the interactions between the electrons. The temperature dependence of the a term is derived from the Fermi factors in band theory, treating the excitations as uncorrelated electron-hole pairs:

$$a(T) = \frac{1}{\chi_0}\left(1 + \frac{T^2}{T_F^2}\right) \tag{5}$$

where χ_0 is the non-interacting (Pauli) susceptibility and T_F is an effective degeneracy temperature (Lonzarich and Taillefer 1985). The b coefficient is only weakly temperature dependent. Differentiating with respect to M gives the magnetic equation of state:

$$\frac{1}{V}\frac{\partial F}{\partial M} = B = (a - I)M + bM^3 + \cdots \tag{6}$$

where B is the magnetic field. The susceptibility χ is then given by

$$\chi = \left.\frac{\partial M}{\partial B}\right|_{M\to 0} = \frac{1}{a - I}.$$

It follows that the onset of ferromagnetism occurs when χ diverges, i.e. $a - I = 0$, which leads to a value for the ordering temperature T_0:

$$T_0 = T_F(I\chi_0 - 1)^{1/2}. \tag{7}$$

In practice this estimate for T_C from realistic band structures can be too large by a factor of ten or more. Moreover the form of the susceptibility in the paramagnetic state ($T > T_0$) is found to be:

$$\chi = \frac{\chi_0}{(I\chi_0 - 1)}\frac{T_0^2}{T^2 - T_0^2},$$

whereas experimentally it is more usual to find a Curie-Weiss law:

$$\chi = \frac{N\mu_B^2\mu_{\text{eff}}^2}{3k_B(T - T_C)}. \tag{8}$$

For itinerant magnets the value of the effective paramagnetic moment μ_{eff} is usually much larger than the low temperature spontaneous moment μ_0 in the ordered state.

The fault with Stoner theory is that it ignores the effects of the correlations between the electron-hole pair excitations (i.e. spin fluctuations) and their effects in renormalising the one-electron density of states. Early attempts to include the spin fluctuation contribution to the free energy (known as "paramagnon" theories, named after the sharply peaked structure in the spectral density (Figure 1)) derived the contributions to the heat capacity (Doniach and Englesberg 1966 and Berk and Scrieffer 1966). When this approach is applied to ferromagnets, however, it is found that the RPA dynamical susceptibility still diverges at T_0 in the static long wavelength limit, while the ordering temperature T_C is renormalised to a value below T_0. There is a lack of consistency between the RPA susceptibility and that calculated from the renormalised free energy.

2 Self-consistent renormalisation of spin fluctuations

Self consistent theories were first introduced by Murata and Doniach (1972) and by Moriya and Kawabata (1973). The Self-Consistent Renormalisation (SCR) theory of spin fluctuations has been developed from these by Moriya (1985) and has been extended and applied to a number of weak ferromagnets by Lonzarich and Taillefer (1985). We stay close to the latter treatment in the following. The basic approach is to add a term $\Delta F(M)$ to the free energy (Equation 4) which comprises a sum over thermally populated spin fluctuation modes, calculated in the presence of an applied field which stabilises the magnetisation M. Taking the classical approximation for the detailed balance factor $[\exp(\hbar\omega/k_BT) - 1]^{-1} \approx k_BT/\hbar\omega$ in Equation (3) leads to:

$$\langle m_\nu^2 \rangle = \frac{k_BV}{T} \sum_q \frac{1}{\pi} \int_{-\infty}^{\infty} \frac{\text{Im}\,\chi_\nu(q,\omega)}{\omega}\, d\omega = \frac{k_BT}{V} \sum_q \chi_\nu(q) \tag{9}$$

This follows from the Kramers-Kronig relation between the real and imaginary parts of the susceptibility. The free energy then has the form:

$$\frac{F(M)}{V} = \frac{F_0(0)}{V} + \frac{aM^2}{2} + \frac{bM^4}{4} + \frac{k_BT}{2V} \sum_{\nu,q<q_c} \ln[\chi_\nu^{-1}(q)] \tag{10}$$

The interaction term $-IM^2/2$ has been incorporated into the quadratic term, to give a single parameter a. Differentiating with respect to M leads to the equation of state

$$\frac{1}{V}\frac{\partial F}{\partial M} = B = \left[a + b\left(3\langle m_\parallel^2 \rangle + 2\langle m_\perp^2 \rangle\right)\right] M + bM^3 \tag{11}$$

where $\langle m_\parallel^2 \rangle$ and $\langle m_\perp^2 \rangle$ are the mean square amplitudes of the spin fluctuations parallel and perpendicular to the direction of the mean magnetisation M. The temperature dependence of the last term in (10) and of the spin fluctuation amplitudes in (11) are much stronger than that of the $a(T)$ term (5). The self-consistency of the equation of state given by equations (9), (10), (11) is simplified by taking the long wavelength limit for $\chi_\nu(q)$:

$$\chi_\nu^{-1}(q) = \chi_\nu^{-1} + cq^2 + \cdots \qquad \text{where} \quad \chi_\parallel^{-1} = \frac{\partial B}{\partial M} \quad \text{and} \quad \chi_\perp^{-1} = \frac{B}{M}$$

The cut-off wavevector q_c in (10) increases with temperature in line with the number of thermally populated spin fluctuation modes. The low frequency approximation for the dynamical susceptibility in the paramagnetic state reduces to

$$\chi^{-1}(q,\omega) = \chi^{-1}(q)\left(1 - \frac{i\omega}{\Gamma(q)}\right) \tag{12}$$

where for a ferromagnet

$$\Gamma(q) = \gamma q \chi^{-1}(q) \tag{13}$$

The cut-off wavevector may then be defined from $\hbar\Gamma(q_c) = k_B T$.

In summary, once we have made the long wavelength and low frequency approximation for the susceptibility, the magnetic equation of state may be determined self consistently in terms of only four parameters, namely a, b, c and γ. Two of these parameters, a, b may be found from the zero temperature equation of state (and hence from a model of the band structure) while the c and γ are determined from inelastic neutron scattering experiments, as described below.

The Curie temperature T_C in SCR theory is found to be smaller than the Stoner value T_0. To see this we consider the approach to T_C from the paramagnetic phase, in which $\langle m_\parallel^2 \rangle = \langle m_\perp^2 \rangle = \langle m^2 \rangle / 3$. At T_C, $\chi_\nu^{-1} = 0$, so that $\chi_\nu^{-1}(q) = \chi_\nu^{-1} + cq^2 + \cdots \approx cq^2$ and also $\Gamma(q) = \gamma q \chi^{-1}(q) \approx \gamma c q^3$. It follows that the cut-off wavevector is $q_c = (k_B T/\hbar\gamma c)^{1/3}$. The condition for T_C is that the coefficient of the linear term in the equation of state vanishes, i.e.

$$a\left(\frac{T^2}{T_0^2} - 1\right) + \frac{5}{3} b \langle m^2 \rangle = 0. \tag{14}$$

Then from (9) we have

$$\langle m^2 \rangle = \frac{3k_B T}{V} \sum_q \chi(q) = \frac{3k_B T}{(2\pi)^3} \int_0^{q_c} \frac{1}{cq^2} d^3q = \frac{3k_B T q_c}{2\pi^2 c}. \tag{15}$$

Equation (14) now be written in the form:

$$1 - \frac{T_C^2}{T_0^2} - \frac{T_C^{4/3}}{T_1^{4/3}} = 0 \tag{16}$$

where

$$T_1 = \left(\frac{2\pi^2 a}{5b}\right)^{3/4} \frac{c(\hbar\gamma)^{1/4}}{k_B}.$$

In the limit where $T_1 \ll T_0$, when the spin fluctuations dominate the temperature dependence of the equation of state, the Curie temperature T_C is equal to T_1, and is then determined by all four parameters a, b, c and γ. The ratio a/b is equal to the square of the spontaneous magnetisation M_0^2 at low temperatures. When experimental values of M_0 , c and γ are inserted, it is found that the Curie temperatures of weak ferromagnets are given with remarkable accuracy by SCR theory. For example $T_C^{\text{calc}} = 31\text{K}$ for MnSi, compared to the measured value of 29.5K, while for Ni_3Al the corresponding values are 39K and 41K respectively (Lonzarich and Taillefer 1985 and Moriya 1985).

From equation of state (11) the uniform susceptibility in the paramagnetic phase is the reciprocal of the term linear in M (since $\chi = (\partial M/\partial B)_{M\to 0}$). It follows that

$$\chi^{-1}(T) = a\left(\frac{T^2}{T_0^2} - 1\right) + \frac{5}{3}b\langle m^2\rangle. \tag{17}$$

The dominant temperature dependence here comes from the mean square amplitude of the spin fluctuations $\langle m^2\rangle$, which from (15) increases like T (or, close to T_C, like $T^{4/3}$, allowing from the temperature dependence of q_c in (15)). It follows that the susceptibility shows a temperature dependence close to Curie-Weiss behaviour (8), with some deviations for temperatures near T_C. The ratio of $\mu_{\rm eff}/\mu_0$ is found to be large, in agreement with experiment (Lonzarich and Taillefer 1985 and Moriya 1985).

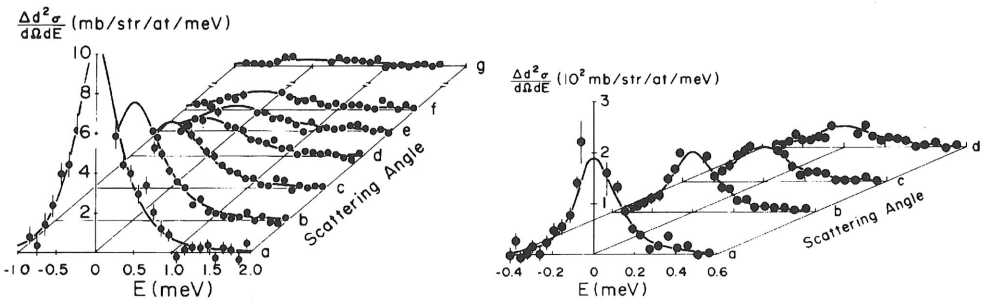

Figure 2. *Inelastic neutron cross sections for the exchange enhanced paramagnet Ni_3Ga (left) and the weak ferromagnet $ZrZn_2$ (right) in the paramagnetic phase (Lonzarich et al. 1989 and Bernhoft et al. 1983). The full lines are fits to the SCR theory from which the parameters c and γ are derived.*

3 Inelastic neutron scattering studies

The inelastic neutron cross section is proportional to the dynamic structure factor

$$S(q,\omega) = \frac{n(\omega)+1}{\pi}\,\mathrm{Im}\,\chi(q,\omega) \tag{18}$$

where $\hbar\omega$ is the energy transfer and q is the wavevector transfer in the scattering process. From (12) we have in the paramagnetic state:

$$\frac{1}{\omega}\,\mathrm{Im}\,\chi(q,\omega) = \frac{\chi(q)\Gamma(q)}{\omega^2 + \Gamma(q)^2}, \tag{19}$$

i.e. the lineshape is Lorentzian with the linewidth $\Gamma(q)$ given by (13). This form for the cross section appears to be an excellent description of real systems in the limit of small ω and q. Figure 2 show the measured cross section in the paramagnetic state for the weak ferromagnet $ZrZn_2$ and the exchange enhanced paramagnet Ni_3Ga (Lonzarich *et al.* 1989 and Bernhoft *et al.* 1983). The lines in the figures are fits to the cross section using (16) with $c = 3\times10^5$Å^2, $\hbar\gamma = 1.8\mu$eV-Å for $ZrZn_2$ and $c = 1\times10^5$Å^2, $\hbar\gamma = 3.0\mu$eV-Å for

Ni_3Ga. Some of the most extensive inelastic neutron measurements have been made on MnSi. This compound orders below 29.5K with a long wavelength (180Å) helical magnetic structure. A magnetic field of only 0.6T is sufficient to induce a ferromagnetic state in which the Mn atoms carry a moment of 0.4μB. Figure 3 shows contours of the scattering measured at two temperatures in the paramagnetic state, one just above T_N, the other close to room temperature (Ishikawa *et al.* 1985). This shows clearly the increase in the cross section, due to the increase in amplitude of the spin fluctuations with temperature.

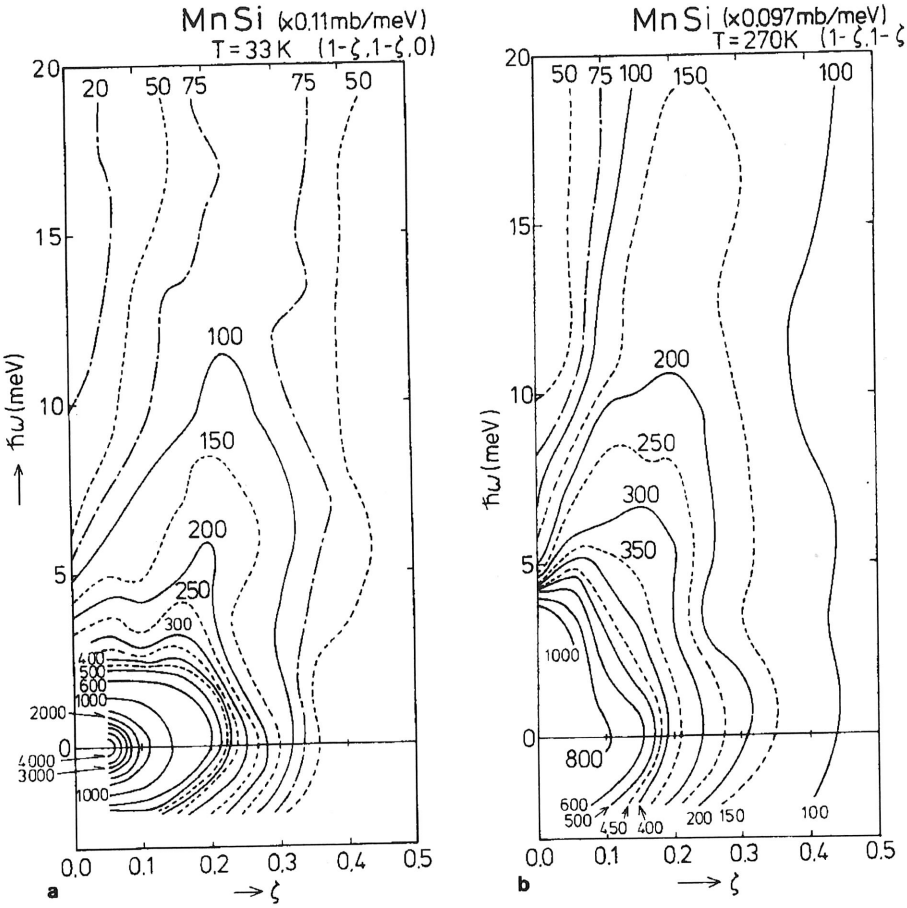

Figure 3. *Contours of neutron scattering cross section for MnSi in the paramagnetic state at two temperatures: (a) 33K, just above T_C and (b) 270K (Ishikawa et al. 1985).*

The linewidth $\Gamma(q)$ for MnSi in the paramagnetic state is shown plotted against the function $q(q^2 + \kappa^2)$ in Figure 4, where $\kappa = (c\chi)^{-1/2}$ is the inverse correlation length (Ishikawa *et al.* 1985). This plot shows that the linewidth is consistent with the form of (13) and the small q expansion of $\chi(q)$. These data, together with experiments on the weak ferromagnet Ni_3Al, and the enhanced paramagnets $TiBe_2$ and YCo_2, verify that the SCR theory gives a good account of the spin dynamics of these classes of itinerant magnets.

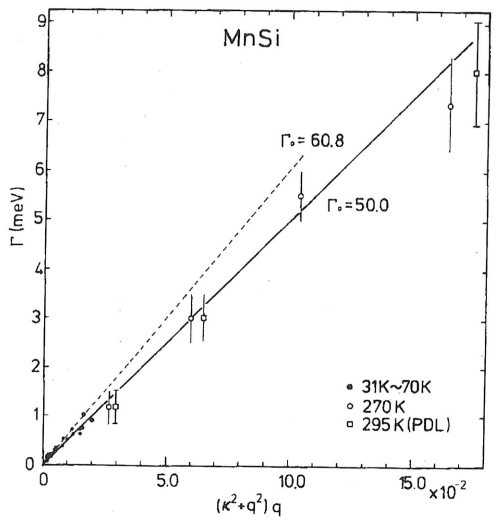

Figure 4. *Line-width $\Gamma(q)$ for MnSi plotted against $q(\kappa^2 + q^2)$ at different temperatures [cf Equation (13)], where κ is the measured inverse correlation length (Ishikawa et al. 1985).*

4 Muon spin relaxation measurements

In a longitudinal geometry experiment the μSR relaxation rate due to fluctuating local magnetic fields is

$$\lambda = G \sum_{\alpha=x,y} \int_0^\infty \langle B_\alpha(0) B_\alpha(t) \rangle \, dt$$

where the coupling constant G depends on whether we are dealing with hyperfine or dipolar interactions. Assuming that the local fields are mainly due to the fluctuating spins on nearby magnetic atoms we can put

$$B_\alpha(t) = \sum_{m,\beta} D_{\alpha\beta}(m) S_m^\beta(t)$$

where the $D_{\alpha\beta}$ coefficient describes either the dipolar or hyperfine coupling mechanism. The relaxation rate then becomes:

$$\lambda = G \sum_{\alpha,\beta} \sum_{m,n} D_{\alpha\beta}(m) D_{\alpha\beta}(n) \int_0^\infty dt \langle S_m^\beta(0) S_n^\beta(t) \rangle.$$

Inserting the spatial Fourier transforms

$$S_q(t) = \sum_m e^{-iqm} S_m(t),$$

it is straightforward to show that

$$\lambda = G \frac{1}{N} \sum_q |D(q)|^2 \int_0^\infty \langle S_{-q}(0) S_q(t) \rangle dt = \frac{\pi G}{N} \sum_q |D(q)|^2 S(q,0), \qquad (20)$$

where $S(q,0)$ is the zero frequency limit of the dynamical structure factor $S(q,\omega)$ and $D(q)$ is the Fourier transform of $D_{\alpha\beta}(m)$, summed over α, β. Then from (15) and (16)

$$S(q,0) = \lim_{\omega\to 0}\left[\frac{n(\omega)+1}{\pi}\mathrm{Im}\,\chi(q,\omega)\right] = \frac{k_B T\chi(q)}{\pi\Gamma(q)}. \tag{21}$$

The μSR relaxation rate therefore can give extra information about the coefficients c and γ which occur in the SCR theory. Rather surprisingly the only detailed μSR work on weak ferromagnets has been that carried out on MnSi (Hayano *et al.* 1978). This was some of the first work to be carried out using the zero field μSR technique. The temperature dependence of the relaxation rate in the paramagnetic phase of MnSi was found to be $\lambda(T) \sim T/(T-T_C)$, as shown in Figure 5 (Hayano *et al.* 1978). This follows directly from the form for $\Gamma(q)$ in (13) and the small q expansion of $\chi(q)$. If we ignore the q dependence of $D(q)$ then

$$\lambda = G\frac{k_B T}{N}\sum_q \frac{\chi(q)}{\Gamma(q)} \approx \frac{4\pi G k_B T}{\gamma}\int \frac{q\,dq}{(\chi^{-1}+cq^2)^2} = \frac{4\pi G k_B T\chi}{c\gamma}\frac{q_m^2}{q_m^2+\kappa^2}$$

where q_m is the upper limit of the wavevector and $\kappa^2 = (\chi c)^{-1}$. It follows that if the uniform susceptibility χ has the Curie Weiss form (8), then $\lambda \approx T/(T-T_C)$.

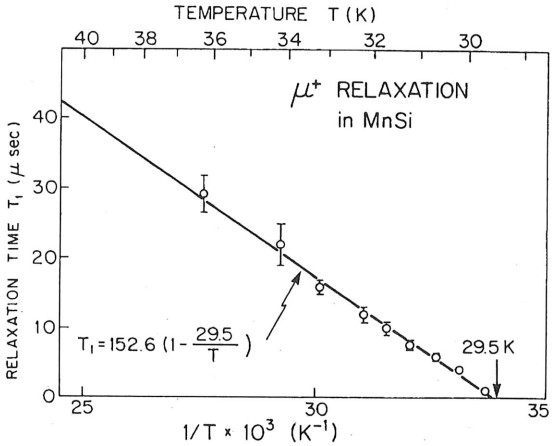

Figure 5. *Temperature dependence of inverse of μSR relaxation rate $\lambda^{-1} = T_1$ for MnSi above T_C (Hayano et al. 1978). The linear plot versus T^{-1} shows that $\lambda \propto T/(T-T_C)$ with $T_C = 29.5$K.*

Later work on MnSi has included a study of the nuclear quadrupole splitting of the ^{55}Mn nucleus via avoided level crossing resonance (ALCR) spectroscopy (Kadono *et al.* 1993). Two resonances were observed since $I = 5/2$ for ^{55}Mn. The quadrupolar splittings were found to be quite strongly temperature dependent, suggesting that in MnSi there is an interaction between the charge density and the spin density that couples the electric field gradient to the critical fluctuations. Further work on the muon spin relaxation has concentrated on the muon-nuclear double relaxation effects (Kadono *et al.* 1990).

It is somewhat surprising that other weak ferromagnets and exchange enhanced paramagnets have not been studied by μSR in a systematic way, especially since μSR data

is obtained far more readily than a detailed neutron investigation, which would have to cover a range of (q, ω) space at each temperature. μSR is also sensitive to a different time/frequency domain from neutron scattering. Any departures from the SCR predictions, which might show up in μSR data, would give important insight into the dynamical scaling in these materials.

5 Fluctuations in antiferromagnets

The main feature of systems showing antiferromagnetic spin fluctuations is that the susceptibility $\chi(q)$ is peaked in the vicinity of an ordering wavevector Q which may be either commensurable or incommensurable with the lattice. The former case leads to a simple antiferromagnet below the Néel temperature (at which $\chi(Q)$ diverges), while incommensurable wavevectors lead to a modulated magnetic structure (helical or sinusoidal) below T_N. The uniform susceptibility $\chi(0)$ is often quite featureless, while in the vicinity of the ordering wavevector $\chi(q)$ can be expanded as above:

$$\chi^{-1}(Q+q) = \chi_Q^{-1} + cq^2 + \cdots = \chi_Q^{-1}(1 + q^2/\kappa^2). \tag{22}$$

Within SCR theory the most distinct contrast to the ferromagnetic case is in the q dependence of the linewidth $\Gamma(q)$. For antiferromagnets Moriya and Hasegawa (Hasegawa and Moriya 1974) have shown that

$$\Gamma(q) = \gamma(q^2 + \kappa^2), \tag{23}$$

so that the linewidth goes to a finite value $\gamma\kappa^2$ at $q = 0$, unlike the ferromagnetic case. The different q dependence of Γ leads to a different result for the temperature dependence of the μSR relaxation rate λ. From equations (20) and (21) above it is straightforward to show that λ scales like $\chi_Q T_\kappa$, to leading order. Since $\kappa = (\chi_Q c)^{-1/2}$ then we would expect $\lambda \approx T/(T - T_N)^{1/2}$, when the staggered susceptibility displayed Curie-Weiss behaviour. This means that λ tends to increase with temperature like $\sqrt{T}$ for $T \gg T_N$ (Moriya 1985).

Perhaps the mostly widely studied systems that display antiferromagnetic spin fluctuations are YMn_2 and β-Mn . Their extraordinary magnetic properties result from a rather unique combination of circumstances, namely the proximity of the itinerant electron system to moment instability (YMn_2) or moment formation (β-Mn), together with the topological frustration arising from antiferromagnetic correlations on lattices of corner sharing tetrahedra (YMn_2) or triangles (β-Mn). Both of these systems show large amplitude spin fluctuations and a great sensitivity of the magnetic properties to the unit cell volume. In studies of these systems microscopic probes like NMR, μSR and neutron scattering have contributed a great deal. In the following we would like to stress the complementarity of inelastic neutron scattering and μSR techniques.

6 YMn_2 and related alloys

YMn_2, which has the C15 cubic Laves structure, displays a dramatic first order phase transition to an antiferromagnetically ordered state at 100K, which is accompanied by a

5% increase in cell volume (Shiga 1988). This AF transition is suppressed completely by a pressure of only 0.4Gpa, or by the substitution of 2% of Y by Sc or of 2.5% of Mn by Fe. In these cases the ground state appears to be very similar to the spin liquid ground state of β-Mn, which shows no sign of magnetic order down to low temperatures. Substitution of Mn by Al in both β-Mn and YMn_2 tends to stabilise a local moment on the Mn atoms, and causes a reduction of the magnetovolume effects.

6.1 Neutron scattering studies of YMn_2

Neutron scattering studies of YMn_2 have been carried out by a number of groups, mostly using neutron polarisation analysis (PA) to separate the spin fluctuation response from the phonon scattering [Deportes *et al.* 1987a,b and Feltoft *et al.* 1988]. The PA technique has the disadvantages that count rates are low compared to unpolarised neutron spectrometers and it is necessary to scan point by point in $(\mathbf{K},\omega)$ space. We chose instead to use time-of-flight spectroscopy with unpolarised neutrons, allowing spectra to be collected over a wide range of K and ω simultaneously (Rainford *et al.* 1992). The separation of the magnetic response from the phonon scattering was effected by extrapolating the measured signal from high K values, where the magnetic form factor $f^2(K)$ is small, to lower K values. The form of this extrapolation was established by extensive Monte Carlo simulations of the multiple phonon scattering. Details of the procedure are given in the reference by Rainford *et al.* 1992. The method is particularly well suited to systems with antiferromagnetic correlations where the integrated magnetic response $\chi(K)f^2(K)$ peaks strongly at intermediate values of K. Constant K cuts through the (K,ω) scattering surface were well represented by a Lorentzian lineshape function:

$$\frac{\mathrm{Im}\,\chi(K,\omega)}{\omega} = \chi(K)\frac{\Gamma}{\Gamma^2+\omega^2} \tag{24}$$

For the incident energies used (60 to 100meV) energy transfers could be measured out to 40–50meV in the K range between 1Å^{-1} and 3Å^{-1}, where the magnetic scattering peaks. In all the samples studied, namely pure YMn_2 and four alloys with 4% Fe, 3% Al and 10% Al substitution for Mn, and 3% Sc substitution for Y, there was still significant scattering out to the edge of the accessible (K,ω) domain (Dakin 1993). It follows that there is a component of the spin fluctuation response extending out to high frequencies. It should be noted that measurements on polycrystalline samples involve a spherical (powder) average over the direction of the scattering vector $\mathbf{K}$, so that the simple lineshape (24) masks the detailed dependence of the linewidth Γ on the wavevector q. However the wavevector-dependent susceptibility $\chi(K)$ can be derived directly from the lineshape (24) using the Kramers-Kronig relations.

Figure 5 shows $\chi(K)$ as a function of temperature derived in this way for the alloy $Y(Mn_{0.96}Fe_{0.04})_2$. The susceptibility was placed on an absolute scale by normalisation of the scattering against the incoherent scattering of a standard vanadium sample. The substitution of 4% Mn by Fe contracts the unit cell of YMn_2 and suppresses the first order transition. This allows measurements of the spin fluctuation response to be made down to low temperatures. It can be seen that there is substantial temperature dependence to (K): the peak response doubles between 200K and 4K, and at the lower temperatures a double-peaked structure develops. In our earlier paper (Rainford *et al.* 1992) we analysed this

data assuming that the characteristic wavevectors of the spin fluctuations were close to the reciprocal lattice vectors of the antiferromagnetically ordered phase of YMn_2, namely τ_{110}, τ_{210}, τ_{211}, *etc.* Recent important measurements on single crystals of YMn_2 have shown that this is not the case. Ballou *et al.* (1996), using a triple axis spectrometer, showed that the magnetic response peaks in kidney-shaped blobs displaced from τ_{110} towards the corner of the Brillouin zone at $(Q,Q,0)$ with $Q \approx 1.25$ (Figure 2, left). We have now reanalysed the $\chi(K)$ data in the light of this new information (Rainford *et al.* 1998). The solid lines in Figure 6 are fits to a model for the spherically averaged form of $\chi(\mathbf{q})$ in which the form of the susceptibility was taken, for simplicity, to be a Gaussian function of q centred on $\tau_{\mathbf{Q}} = (Q,Q,0)$ type positions ($\mathbf{q} = \mathbf{K} - \tau_{\mathbf{Q}}$):

$$\chi(\mathbf{q}) = A \exp[-|\mathbf{q}|^2/2\sigma^2] \tag{25}$$

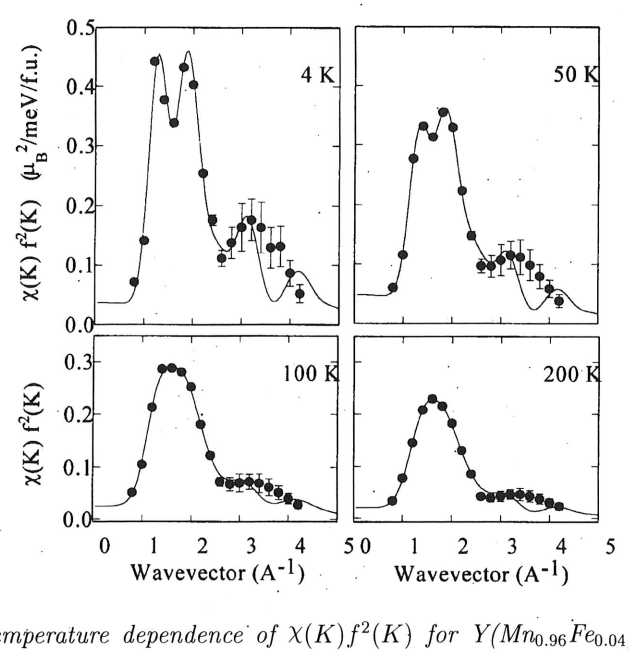

Figure 6. *Temperature dependence of $\chi(K)f^2(K)$ for $Y(Mn_{0.96}Fe_{0.04})_2$ derived from inelastic neutron spectra. The solid lines are a fit to a model of the powder average of $\chi(q)$ as discussed in the text (Rainford et al. 1998).*

The equivalent positions were derived from a Brillouin zone doubled in each direction, namely zone centres at (2,2,2), (4,0,0), (4,4,0) etc., plus all equivalent vectors $(Q,Q,0)$. The doubling of the Brillouin zone required to describe the characteristic wavevectors found in the single crystal measurements implies that the antiferromagnetic correlations are strongest within a subunit of the unit cell, most likely a single tetrahedron of four nearest neighbour Mn atoms. The form of the spherical average of $\chi(\mathbf{q})$ used in the fits is given in reference (Rainford *et al.* 1992). The values of Q found in the fits in Figure 6 ranged from 1.13Å^{-1} at 4K to 1.21Å^{-1} at 200K, somewhat smaller than the value 1.25Å^{-1} found for YMn_2 in the single crystal data (Rainford *et al.* 1992). The Gaussian width σ of the $(Q,Q,0)$ peak increased smoothly from 0.19Å^{-1} at 4K to 0.26Å^{-1} at 200K, reflecting

a decrease in the correlation length of the magnetic short range order with increasing temperature. Similar quality fits were obtained for all the alloys measured, though there were some striking qualitative differences in the forms of $\chi(K)$. The $Y_{0.97}Sc_{0.03}Mn_2$ alloy might be expected to give results very similar to those of Figure 6, since Sc substitution contracts the unit cell by a similar amount and suppresses the first order AF transition. However we found that $\chi(K)$ for this alloy is practically independent of temperature and does not show the double peaked structure at low temperature. This suggests magnetic correlations of a shorter range than for the 4%Fe alloy. The two samples with 3 and 10% Al substituted for Mn developed double peaked structure at temperatures as high as 100K. Substitution of Mn by Al expands the cell volume, tending to stabilise the Mn moment. The $\chi(K)$ data are consistent with this picture.

6.2 Evidence for frustration in the spin correlations

Frustration is thought to play a key role in determining the magnetic properties of YMn_2 and its alloys, since the main feature of the magnetism is antiferromagnetic coupling between Mn atoms on a pyrochlore lattice of corner sharing tetrahedra. There has been considerable interest in frustrated localised magnets recently which has led to extensive Monte Carlo simulations for classical spins on the pyrochlore lattice. Reimers (1992) presented powder average $S(K)$ data for the pyrochlore lattice for nearest neighbour exchange which has a form remarkably similar to the high temperature data in Figure 6, corresponding to short range order on a scale of the order of one unit cell. The inclusion of a small amount of second neighbour exchange gives a multiple peaked structure, similar to the low temperature data in Figure 6. The correlations in this case extend out to two or three unit cells. Zinkin and Harris (1995) have used a local mean field approach to calculate the form of $S(\mathbf{q})$ throughout the Brillouin zone (BZ) for the pyrochlore lattice with nearest neighbour exchange. For the (1,-1,0) plane of the BZ the contours of $S(\mathbf{q})$ extend out from the narrow necks along the [h,h,0] directions towards the corners of the BZ at (5/4, 5/4, 0) type positions. These positions are precisely where the scattering is found to peak in the single crystal data for YMn_2. The match is not perfect: when plotted over several Brillouin zones the $S(\mathbf{q})$ data has the appearance of a pattern of "bow-tie" shapes (Figure 7, right), whereas the "kidney" shapes of the YMn_2 data contours (Figure 7, left) are elongated along the BZ boundaries. It would appear then that the distinctive wavevectors associated with the spin fluctuations in YMn_2 are characteristic of the frustrated correlations on the pyrochlore lattice. Canals and Lacroix (1998) have recently shown, using exact diagonalisation of clusters, that the peaks in the neutron cross section at (5/4, 5/4, 0) type positions are also found in the ground state for quantum spins $S = 1/2$ on the pyrochlore lattice.

6.3 Effects of alloying on the spin dynamics of YMn_2

The inelastic neutron spectra from the single crystal samples of $Y_{0.97}Sc_{0.03}Mn_2$ and YMn_2 (Rainford *et al.* 1992) are well described by a Lorentzian lineshape (19), though there is not much published information so far about the form of $\Gamma(q)$ or its temperature dependence, except that the linewidth varies slowly with wavevector. We have attempted to extract further information about Γ from the time-of-flight data on polycrystalline samples by

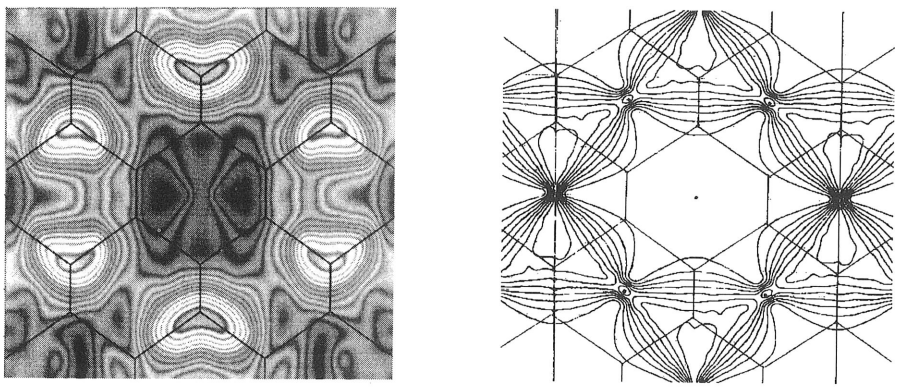

Figure 7. *Left: contours of scattering from spin fluctuations in Y(Sc)Mn_2 in (1,-1,0) plane of the BZ, after (Ballou et al. 1996). (right): Contours of $S(\mathbf{q})$ in the (1,-1,0) plane of the BZ for the pyrochlore lattice with nearest neighbour exchange, after (Zinkin and Harris 1995). In both plots the BZ boundaries are overlaid. The [001] direction is horizontal and the [110] direction is vertical.*

fitting the constant K cuts through the data to a powder average of (19). In order to do this we assumed the form for $\Gamma(q)$ given in (23) and further assumed the form for $\chi(q)$ given by the small q expansion:

$$\chi(q) = \frac{\chi\kappa^2}{(\kappa^2 + q^2)} \tag{26}$$

Together these give an analytic form for the powder average lineshape function, which can be fitted to the constant K cuts. The results for the linewidth $\Gamma(0)$ derived from the fits are shown in Figure 8 (Rainford *et al.* 1995). The filled symbols are derived from the neutron data on YMn_2 (squares), and the alloys with 4%Fe (diamonds), 3%Al (inverted triangles) and 10% Al (triangles) substitution for Mn, and 3%Sc (circles) substitution for Y. It is clear that the expansion of the unit cell volume by Al substitution decreases the linewidth, while the contraction of the unit cell in Y(Sc)Mn_2 and Y$(MnFe)_2$ increases the linewidth.

μSR measurements also give direct information about the spin dynamics. In studies of YMn_2 and $YMn_{1.94}Fe_{0.06}$ (Cywinski *et al.* 1990, 1991) the muon relaxation rate increases as the temperature is lowered, diverging close to T_N in the case of YMn_2 and following a power law dependence for the 3% Fe alloy, where the magnetic order has been suppressed. This is evidence for slowing down of the spin fluctuations. From (20)and (21) above the muon relaxation rate is

$$\lambda = \frac{Gk_BT}{N} \sum_q \frac{\chi(q)}{\Gamma(q)} \tag{27}$$

where again we have ignored the q dependence of the $D(q)$ factor. In practice we do not have detailed information about $\chi(q)$ or $\Gamma(q)$, but it would appear from the inelastic neutron data on single crystals that the wavevector dependence of the linewidth $\Gamma(q)$ is rather weak. In this case we may rewrite (27) as

$$\lambda = \frac{Gk_BT\chi_L}{\Gamma}, \tag{28}$$

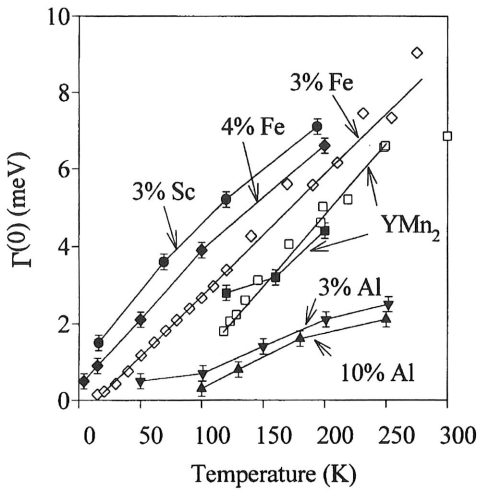

Figure 8. *Linewidth parameter for YMn_2 alloys from fits to inelastic neutron spectra (solid symbols) and from scaled μSR data using Equation (28) (open symbols) (Rainford et al. 1995).*

where χ_L, the local susceptibility, is defined by:

$$\chi_L = \frac{1}{N}\sum_q \chi(q).$$

This may be derived from $\chi(K)$ as described in Rainford *et al.* (1992). We have shown, using this approach, that the systematics of $\lambda(T)$ for YMn_2 and the alloys with Fe substitution agree very well with the neutron linewidths, once a scale parameter (i.e. the coupling constant G) can be determined (Rainford *et al.* 1995). The open symbols in Figure 8 are estimates of the linewidth Γ, derived from the measured μSR relaxation rates λ using (28) for YMn_2 (open squares) and for an alloy with 3%Fe substitution for Mn (open triangles). The temperature dependence of χ_L, the local susceptibility was taken to be Curie-Weiss like, as determined by the neutron measurements (Rainford *et al.* 1992, Dakin 1993), and a single value of the coupling parameter G was used to scale these data to the linewidths derived from the neutron measurements (filled circles). From SCR theory (23) we would expect $\Gamma(0)$ to vary as $\gamma\kappa^2 \approx c\gamma\chi^{-1}$, and this should scale as $(T - T_N)$. This is consistent with the approximately linear behaviour shown in Figure 8. In the case of $YMn_{1.8}Al_{0.2}$ (Cywinski and Rainford 1994) the character of the muon relaxation was rather different, in that the relaxation function was fitted best by a stretched exponential form (Figure 9a):

$$G_z(t) = a_0 \exp\left[-(\lambda t)^{\beta}\right] \tag{29}$$

The exponent β was found to be temperature dependent, tending towards the value 1/3 just above the spin glass temperature T_G. This form has been found in a large number of concentrated spin glass systems, and in this context provides additional confirmation that substitution of Mn by Al tends to stabilise local moments on the Mn. We were able to apply (28) to these data also: the temperature dependence $\Gamma(T)$ was found by Motoya *et al.* (Freltoft *et al.* 1988 and Motoya *et al.* 1988) to follow an Arrenhius law:

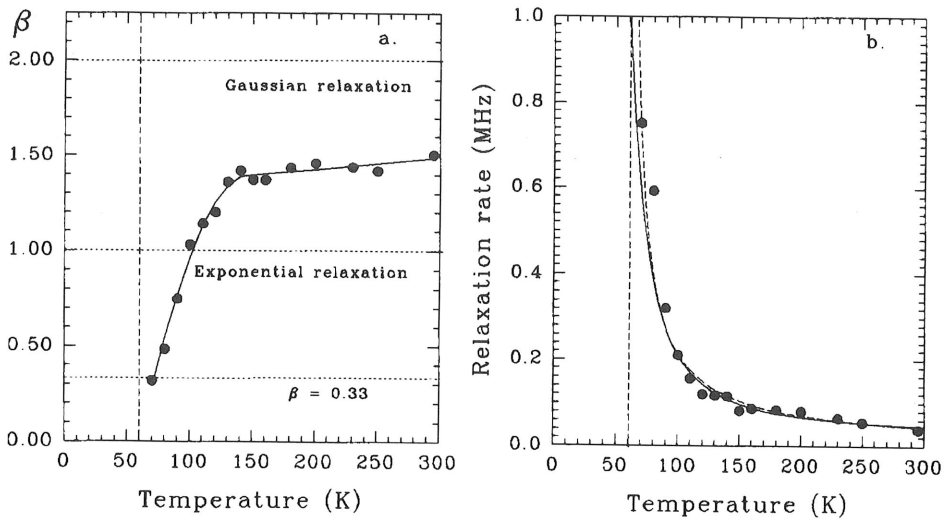

Figure 9. *Temperature variation of (a) the exponent of the stretched exponential (29) and (b) the relaxation rate λfor $Y(Mn_{0.9}Al_{0.1})_2$. The dashed curve in (b) is a fit to a power law behaviour for $\lambda(T)$ with exponent 0.9, while the solid line is the form given by (28) with $\Gamma(T)$ given by an Arrenhius law and $\chi_L(T) = C/(T+\Theta)$ (see text) (Cywinski and Rainford 1994).*

$\Gamma(T) = \Gamma_0 \exp(-E_a/k_BT)$ with $E_a/k_B = 278.4$K, while our time-of-flight data showed that the local susceptibility χ_L followed a Curie-Weiss law $\chi_L = C/(T+\Theta)$ with $\Theta = 93$K. Putting these results into (28) gave a form for $\lambda(T)$ that agreed remarkably well with the experiment (Figure 9b).

7 β-Mn and β-Mn-Al alloys

β-Mn is the only stable allotrope of elemental manganese that does not display a magnetic moment at any temperature. Previous work by Shiga's group has shown convincingly that the magnetic properties of β-Mn are characterised by strong spin fluctuations associated with Mn moments on the verge of localisation (Nakamura *et al.* 1997). The cubic A13 type crystal structure has 20 atoms in the unit cell, with two inequivalent sites. Eight Mn occupy the site with trigonal point symmetry (site I), while the remaining 12 Mn occupy the orthorhombic site II. It appears from NMR and NQR data that the Mn on site I are very weakly magnetic. But the large nuclear spin relaxation rate and high resonance frequency for the site II Mn are consistent with a strong hyperfine field at the nucleus arising from coupling with strong, slow spin fluctuations (Nakamura *et al.* 1997). The similarity with Y(Sc)Mn_2 alloys suggests that geometrical frustration also plays an important role. Nakamura *et al.* (1997) have accounted for the frustration through a description of the type II sites as a network of corner-sharing regular triangles, with similarities to the Kagome lattice.

Inelastic neutron scattering measurements on β-Mn and β-$Mn_{0.9}Al_{0.1}$ have been made

by Nakamura *et al.* (1997) using polarisation analysis. Recent data taken using the time-of-flight method (Stewart 1998, Stewart *et al.* 1999) have provided complementary information for pure β-Mn and for a β-$Mn_{0.8}Al_{0.2}$ alloy. In β-Mn the linewidth of the spectra increases from 20 to 30meV between 7K and 290K; these widths are much larger than those found in YMn_2. Figure 10 shows the temperature dependence of $\chi(K)f^2(K)$ for β-Mn obtained by carrying out energy integration of constant K cuts of the time-of flight data (Stewart 1998, Stewart *et al.* 1999).

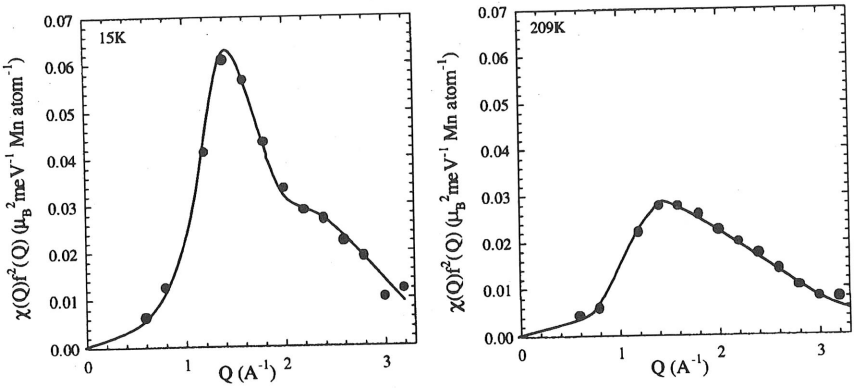

Figure 10. *Integrated response $\chi(K)f^2(K)$ for β-Mn at 15K and 209K (Stewart 1998, Stewart et al. 1999). The solid lines are guides to the eye.*

For wavevectors above 2Å^{-1} most of the K dependence comes from the Mn form factor $f^2(K)$, so that at the lower temperature $\chi(K)$ has a form rather like a liquid structure factor. The sharp double peaked structure found in YMn_2 (Figure 6) is not seen in β-Mn, indicating a shorter correlation length of the spin fluctuations. However, as in YMn_2, the AF correlations in β-Mn persist to high temperatures.

For the 10% Al alloy the linewidth is very much smaller, of order 10meV at 290K, and decreases linearly with temperature. The time of flight data for the 20% Al alloy shows that there are two components in the response at low temperature, a narrow quasi-elastic line (with resolution limited width) and a broad response with a width of order 14meV. The broad component was not seen in the PA data for the 10% alloy (Nakamura *et al.* 1997), presumably because these data were collected with a low incident neutron energy.

The evolution of the spin dynamics in β-$Mn_{1-x}Al_x$ alloys has been studied in zero field longitudinal μSR measurements (Stewart *et al.* 1998, Stewart and Cywinski 1999). For alloys with $0 < x < 0.09$ the form of the relaxation function of the muon polarisation could be described by:

$$G_z(t) = a_0 G_z^{KT}(t) \exp(-\lambda t), \tag{30}$$

where $G_z^{KT}(t)$, the static Kubo-Toyabe (KT) function, accounts for the muon depolarisation due to a distribution of static nuclear dipolar fields. The second term arises from the rapidly fluctuating atomic spins. The KT component was found to be independent of temperature. For pure β-Mn the depolarisation due to the atomic spins was found to be independent of temperature also, with a value of $\lambda = 0.02\text{s}^{-1}$. This is consistent with rapid motional narrowing due to the large, weakly temperature dependent linewidth of the spin fluctuation spectrum of β-Mn. As Al is substituted into β-Mn, λ develops strong

temperature dependence, diverging towards low temperature (Figure 11b). This too is consistent with the neutron studies where the inelastic linewidth is seen to decrease as the temperature is lowered in the Al-substituted β-Mn. The initial asymmetry begins to falls below 60K, finally reaching 1/3 of its high temperature value (Figure 11a). This behaviour indicates quasi-static correlations in the low temperature regime. The transition temperatures determined from the divergence of λ and the loss of asymmetry are shown in the magnetic phase diagram, Figure 13.

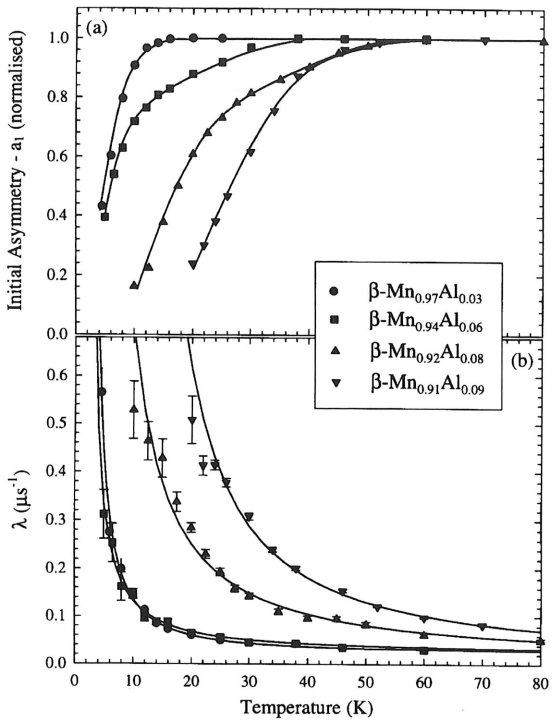

Figure 11. *(a) Initial asymmetry a_0 and (b) relaxation rate λ versus temperature for β-$Mn_{1-x}Al_x$ alloys (Stewart et al. 1998, Stewart and Cywinski 1999) with concentrations $x = 0.03, 0.06, 0.08, 0.09$.*

For Al concentrations above $x = 0.09$ the form of the muon relaxation function changes from the $G_z^{KT}(t)\exp(-\lambda t)$ form to the stretched exponential form $G_z^{KT}(t)\exp[-(\lambda t)^{\beta}]$. The value of β decreases slowly, from 1 at high temperatures to approximately 0.3 at the transition temperature (Figure 12) (Stewart *et al.* 1998, Stewart and Cywinski 1999). As mentioned in Section 6.3, such a response is characteristic of the dynamics in concentrated spin glass systems, and reflects a broadening of the distribution of spin relaxation rates as the spin glass transition T_G is approached. In the concentration regime $0.09 < x < 0.20$ the relaxation rate λ diverges as the temperature is decreased towards T_G (Figure 12). The spin glass transition can also be seen as a sharp drop in the asymmetry at T_G. The magnetic phase diagram (Figure 13) (Stewart *et al.* 1998, Stewart and Cywinski 1999) shows that the spin glass transition temperatures rise rapidly for concentrations above $x = 0.09$. This feature, taken together with the change in form of the relaxation function,

suggests the character of the magnetic ground state changes near 9%Al substitution. The picture emerges that in the low concentration regime ($0 < x < 0.09$), the ground state is a spin liquid, dominated by the zero point spin fluctuations, while above $x = 0.09$ a spin glass state appears, in which the Mn moments are well localised, but still topologically frustrated.

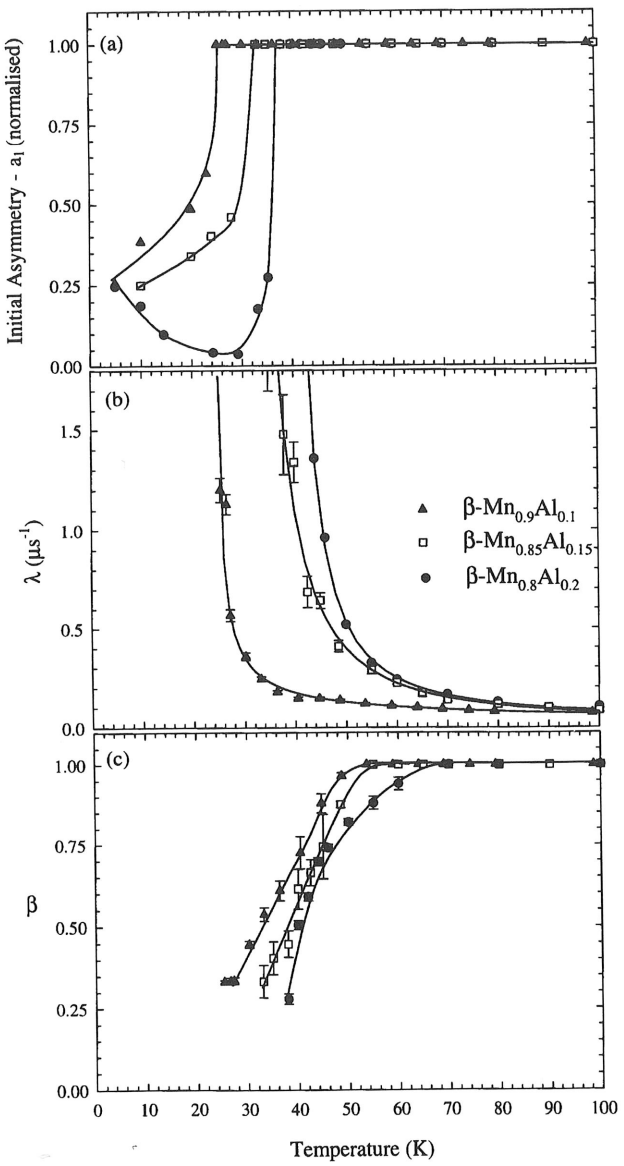

Figure 12. *Temperature dependence of (a) the initial asymmetry, (b) the relaxation rate λ, and (c) the stretch exponent β for β-$Mn_{1-x}Al_x$ alloys with x =0.10, 0.15 and 0.20 (Stewart et al. 1998, Stewart and Cywinski 1999).*

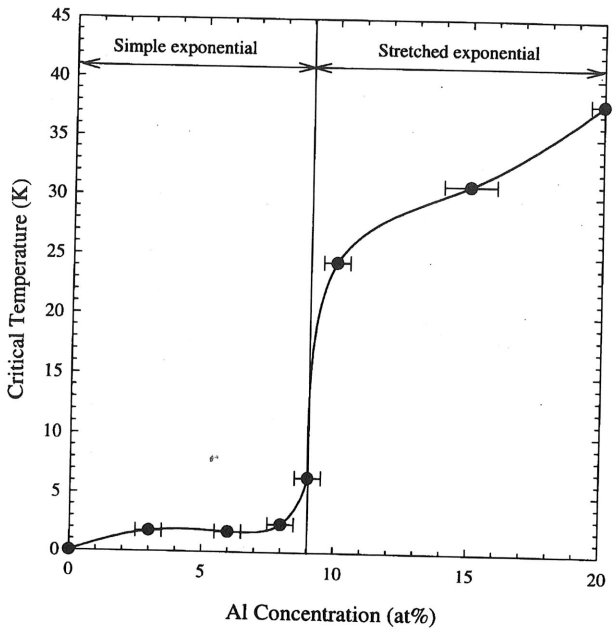

Figure 13. *The magnetic phase diagram for β-$Mn_{1-x}Al_x$ alloys (Stewart et al. 1998, Stewart and Cywinski 1999). The vertical line separates the spin liquid regime $x < 9\%$ from the spin glass regime $x \geq 9\%$.*

8 Conclusions

The SCR theory of spin fluctuations appears to give a full account of the both the static and dynamical properties of weak ferromagnets and exchange enhanced para-magnets. With the exception of the detailed μSR work on MnSi [Hayano *et al.* 1978, Kadono *et al.* 1990, 1993), so far the investigation of the spin dynamics of weak ferromagnets has depended almost entirely on inelastic neutron scattering measurements. It would appear that there is room for further μSR studies in this area, given that μSR data are collected and analysed much more readily than neutron data, and that the muon is sampling a distinct frequency domain from the neutron.

In the cases of YMn_2 and β-Mn alloys there is another dimension to the problem arising from the topological frustration of antiferromagnetically coupled Mn atoms on lattices of corner sharing tetrahedra or triangles. Knowledge of the dynamical response in these materials is crucial for the understanding of the bulk magnetic properties, for example Pinette and Lacroix (1994) have argued that the form of $\chi(\mathbf{q},\omega)$ in $Y(Sc)Mn_2$ leads directly to an explanation of the heavy fermion behaviour found in these alloys. The complementarity of μSR and neutron techniques is well demonstrated by work reported in Sections 6 and 7. Once the scaling between the muon relaxation rate λ, the neutron linewidth Γ and the local susceptibility χ_L has been established, the μSR technique allows the systematics of the spin dynamics to be explored as a function of temperature and alloy composition.

It is still unclear what effect frustration has on the form of the spin dynamics in itinerant magnets. We have argued here that the temperature dependence of the linewidth data in Figure 8 is consistent with SCR theory, which takes no specific account of frustration. However it is well established that for localised spins in frustrating topologies the dynamics are usually dominated by over-damped zero frequency modes. Recent work by Moessner and Chalker (1998) for localised classical spins on the pyrochlore lattice predicts a spin autocorrelation function with an exponential decay in time and a relaxation time that varies as T^{-1}. From (20) this would give a muon relaxation rate λ which diverged as T^{-1}. In the spin liquid phase of β-$Mn_{1-x}Al_x$ alloys ($0.03 \leq x \leq 0.08$) it is found (Stewart *et al.* 1998, Stewart and Cywinski 1999) that $\lambda(T) \approx (T/T_G - 1)^{-\epsilon}$ with values of ϵ in the range 1.1 to 1.3, while in $YMn_{1.94}Fe_{0.06}$ (Cywinski *et al.* 1990) $\lambda(T)$ follows a power law with exponent 0.75. Further theoretical insight is needed into the treatment of frustration in the context of itinerant electron magnetism.

Acknowledgements

I would like to thank Bob Cywinski and Ross Stewart for a very stimulating collaboration and for permission to include unpublished data in this review.

References

Ballou R, Leliévre-Berna E and Fôk, B, 1996, *Physical Review Letters* **76** 2125
Berk N and Schrieffer J R, 1996, *Physical Review Letters* **17** 433
Bernhoeft N R *et al.* , 1983, *Physical Review B* **28** 422
Canals B and Lacroix C, 1998, *Physical Review Letters* **80** 2933
Cywinski R, Kilcoyne S H, Cox S F J, Scott C A and Schaerpf O, 1990, *Hyperfine Interactions* **64** 427
Cywinski R, Kilcoyne S H and Scott C A. 1991, *Journal of Physics: Condensed Matter* **3** 6473
Cywinski R and Rainford B D, 1994, *Hyperfine Interactions* **85** 215
Dakin S J, 1993, PhD Thesis Southampton University (unpublished)
Déportes J, Ouladiaff B and Ziebeck K R A, 1987a, *Journal of Magnetism and Magnetic Materials* **70** 14
Déportes J, Ouladiaff B and Ziebeck K R A, 1987b, *Journal de Physique* **48** 1029
Doniach S and Englesberg S, 1996, *Physical Review Letters* **17** 750
Doniach S, 1967, *Proceedings of the Physical Society* **91** 86
Freltoft T, Böni P, Shirane G and Motoya K, 1988, *Physical Review B* **37** 3454
Hasegawa H and Moriya T, 1974, *Journal of the Physical Society of Japan* **36** 1542
Hayano R S, Uemura Y J, Imazoto J, Nishida N, Yamakazi T, Yasuoka H, and Ishikawa Y, 1978, *Physical Review Letters* **41** 1743
Ishikawa Y, Noda Y, Uemura Y J, Majkrzak C F and Shirane G, 1985, *Physical Review B* **31** 5884
Kadono R Matsuzaki T, Yamazaki T, Kreitzman S R and Brewer J H, 1990, *Physical Review B* **42** 6515
Kadono R, Brewer J H, Chow K, Kreitzman S R, Niedermayer Ch, Riseman T M and Schnieder J W, 1993, *Physical Review B* **48** 16803
Lonzarich G G and Taillefer L, 1985, *Journal of Physics C* **18** 4339
Lonzarich G G, Bernhoeft N R and Paul D McK, 1989, *Physica B* **156, 157** 699

Moessner R and Chalker J T, 1998, *Physical Review Letters* **80** 2929
Moriya T and Kawabata A, 1973, *Journal of the Physical Society of Japan* **34** 639
Moriya T, 1985, "Spin fluctuations in Itinerant Electron Magnetism", Springer Verlag
Motoya K, Freltoft T, Böni P and Shirane G, 1988, *Physical Review B* **38** 4796
Murata K K and Doniach S, 1972, *Physical Review Letters* **29** 285
Nakamura H, Yoshimoto K, Shiga M, Nishi M and Kakurai K, 1997, *Journal of Physics: Condensed Matter* **9** 4701
Pinettes C and Lacroix C, 1994, *Journal of Physics: Condensed Matter* **6** 10093
Rainford B D, Dakin S J and Cywinski R, 1992, *Journal of Magnetism and Magnetic Materials* **104–107,** 1257
Rainford B D, Cywinski R, and Dakin S J, 1995, *Journal of Magnetism and Magnetic Materials* **140–144** 805
Rainford B D, Stewart J R, Cywinski R and Dakin S J, 1998, "Itinerant Electron Magnetism: Fluctuation Effects", Wagner D *et al.* (editors), Kluwer
Reimers J N, 1992, *Physical Review* **45** 7287
Shiga M, 1988, *Physica B* **149** 293
Stewart J R, 1998, PhD Thesis, University of St Andrews (unpublished)
Stewart J R, Rainford B D and Cywinski R, to be published
Stewart J R, Hillier A D, Kilcoyne S H, Manuel P, Telling M T F and Cywinski R, 1998, *Journal of Magnetism and Magnetic Materials* **177–181** 602
Stewart J R and Cywinski R, 1999, *Physical Review B* **59** 4305
White R M, 1983, "Quantum Theory of Magnetism", (Chapter 4), Springer Verlag
Zinkin M P and Harris M J, 1995, *Journal of Magnetism and Magnetic Materials* **140–144** 1803